nature communications

Article

https://doi.org/10.1038/s41467-025-64453-4

Climate change is predicted to reduce global belowground ecosystem multifunctionality

Received: 22 June 2024

Accepted: 17 September 2025

Published online: 22 October 2025

Check for updates

Tiancai Zhou[1], Jian Sun[1] ✉, Chongchong Ye[2], Xin Jing[3], Eryuan Liang[1], Xuyang Lu[4], Akira S. Mori[5], Michael E. Meadows[6,7] & Josep Peñuelas[8,9]

Although climate change is known to abruptly shift ecosystem functions in drylands worldwide, the global response of belowground ecosystem multifunctionality (BEMF) to future climate change remains largely unknown. Herein, we use fifteen indicators associated with key ecosystem functions (e.g., belowground productivity, nutrient pools and cycling) to evaluate global BEMF by averaging, principal component analysis, and single-threshold approaches. Our results reveal marked spatial variation in functionality across Köppen climate biomes, indicating that BEMF is higher in polar and continental biomes compared to dry and tropical biomes. We further identify an abrupt shift in global BEMF at a mean annual temperature (MAT) threshold of approximately 16.4 °C. Globally, temperature and soil pH generate strong negative effects on BEMF in MAT ≤ 16.4 °C regions, whereas precipitation and plant species richness positively dominate the dynamics of BEMF in regions where MAT > 16.4 °C. Importantly, we predict ongoing climate change to result in a 20.8% loss of global BEMF under SSP585 by 2100, particularly in temperate and continental biomes. As future climate change is projected to increase, integrating in situ experiments and Earth system models into BEMF-climate studies is critical to the conservation and sustainability of ecosystem functions.

Over the last decade, a growing body of evidence has established that climate change can trigger abrupt shifts in multifunctionality in regional grassland and worldwide dryland ecosystems[1,2], yet these phenomena remain significantly understudied globally. This oversight is particularly critical given the diverse climate-ecosystem interactions across regions and biomes[3]. For instance, while precipitation predominantly influences microbial activities and ecosystem functions in drylands[4,5]—reduction of water availability potentially leads to severe decreases in soil fertility, plant productivity, and loss in species richness[2,6]—temperature plays a more decisive role in shaping the multifunctionality of alpine ecosystems, such as those on the Tibetan Plateau[7]. Our understanding of how climate directly and indirectly affects biodiversity and ecosystem multifunctionality (Fig. S1), especially relevant to soil functions across various global biomes, is urgently needed to guide effective management and conservation strategies in the face of future climate change[3,8].

A recent meta-analysis indicated that water availability creates thresholds in multiple soil biodiversity and functions[9], but whether

[1]State Key Laboratory of Earth System Resources and Environment of Tibetan Plateau, Institute of Tibetan Plateau Research, Chinese Academy of Sciences, Beijing, China. [2]School of Civil Engineering and Geomatics, Southwest Petroleum University, Chengdu, China. [3]State Key Laboratory of Herbage Improvement and Grassland Agro-Ecosystems, and College of Pastoral Agriculture Science and Technology, Lanzhou University, Lanzhou, China. [4]Institute of Mountain Hazard and Environment, Chinese Academy of Sciences, Chengdu, China. [5]Research Center for Advanced Science and Technology, The University of Tokyo, Tokyo, Japan. [6]School of Geography and Oceanographic Sciences, Nanjing University, Nanjing, China. [7]Department of Environmental & Geographical Science, University of Cape Town, Rondebosch, South Africa. [8]CREAF, Cerdanyola del Valles, Barcelona, Spain. [9]CSIC, Global Ecology Unit CREAF-CSIC-UAB, Bellaterra, Barcelona, Spain. ✉e-mail: sunjian@itpcas.ac.cn

https://doi.org/10.1038/s41467-025-64453-4

such a climate-related threshold is expressed in global belowground ecosystem multifunctionality (BEMF), remains uncertain. BEMF constitutes multiple functions that relate to ecosystem productivity (i.e., belowground biomass), nutrient pools and cycling (i.e., soil nutrients, mineralization, decomposition, respiration, etc.). Despite the fundamental role of belowground functions in supporting a vast array of soil organisms and providing multiple ecosystem services[3,10], a global dearth of reliable data severely hampers our understanding of BEMF. Moreover, with the expected intensification of climate change[11], its impact on global biodiversity and permafrost soil carbon stocks is likely to worsen[12–14], making the need for detailed modeling of global BEMF more pressing. Therefore, we aim to characterize the spatial distribution of BEMF across biomes via interpolated global data, determine the existence of climate thresholds, and illuminate the underlying mechanisms. This knowledge is essential for predicting how belowground ecosystems will respond to future climatic shifts and developing strategies to mitigate these impacts[1,2,9].

In this context, our study addresses three critical questions: (i) How does BEMF vary across Köppen climate biomes; (ii) Does BEMF exhibit abrupt shifts along climate gradients; (iii) In the event of a major loss of biodiversity and permafrost carbon after warming[13–15], how might changing climate degrade ecosystem functions. We find that mean annual temperature (MAT), rather than mean annual precipitation (MAP), accompanies an abrupt shift in BEMF at a threshold of ~16.4 °C, and ongoing climate change portends a 20.8% loss of global BEMF under SSP585 by 2100. Our findings offer climate-specific insights into the conservation of ecosystem functions.

Results and discussion

Global patterns of belowground ecosystem multifunctionality

Following references in the Table. S1 and the criteria for selecting ecosystem function data (see the “Methods” section), 15 indicators (Table S2) linked to key ecosystem processes and functions were used to evaluate BEMF at a global scale, including the indicators of belowground net primary productivity (Fig. S2a), belowground living biomass carbon stock density (Fig. S2c), nutrient pools and fluxes indicators (Fig. S3) of soil organic carbon, soil total nitrogen, soil total phosphorus, soil available phosphorus, soil organic carbon/total nitrogen, soil total nitrogen/total phosphorus, cation exchange capacity, soil dissolved organic carbon, microbial biomass carbon, microbial biomass nitrogen, microbial biomass phosphorus, gross nitrogen mineralization rate, and gross nitrogen immobilization rate. These indicators were chosen because they are critical determinants in supporting and regulating ecosystem functions and are the most widely used indicators in multifunctionality studies (Table S1)[1,7]. Additionally, we used the mean value of BEMF based on three approaches (the average approach, principal component analysis (PCA), and the single threshold approach) to evaluate the global spatial pattern of BEMF to ensure robustness.

Globally, BEMF exhibits high spatial variability across the Köppen climate biomes (Fig. 1a). Specifically, the greatest BEMF is observed in polar (0.55), followed by continental (0.48), temperate (0.30), tropical (0.25) systems, and is lowest in dry biomes (0.14, Fig. 1b). These results address our first research question by demonstrating that higher BEMF is found in Arctic biomes, while lower BEMF is observed in dry and tropical biomes. This pattern can be explained by the fact that, despite lower productivity (Fig. S2a and b) and nutrient fluxes (gross nitrogen mineralization and immobilization rates; Fig. S3w and y) in polar and continental ecosystems compared to tropical biomes, the substantial soil nutrient reservoir (soil organic carbon, total nitrogen, and total phosphorus, etc.; Fig. S3a–f) accounts for higher BEMF in these regions. Similarly, previous studies also demonstrated that ecosystem multifunctionality does not imply that all functions are positively correlated in one ecosystem[16,17]. Indeed, global belowground carbon productivity (24.7 ± 5.7 Pg yr^{-1}, mean ± 2 standard error)[18] is much lower than the surface carbon pool in the northern permafrost zone (1035 ± 150 Pg, mean ± 95% confidence interval)[13,19]. Over 30% of global surface soil carbon is stored in permafrost regions (including most polar and continental biomes), accumulated over millennia and stabilized by anoxia, low temperatures, and acidic soil pH[12,13,20]. Low temperature (Fig. S4b) and soil acidification (Fig. S6b) inhibit organic carbon decomposition in these biomes[7], potentially enhancing multiple soil functions (higher nutrient stocks in permafrost)[21]. Moreover, while decomposition rates are higher in tropical (10.2 Pg C yr^{-1}) compared to those in boreal biomes (0.44 Pg C yr^{-1})[22], significant nutrient leaching through runoff and soil infiltration occurs in tropical ecosystems[23], resulting in widespread low soil nutrient pools[24,25]. Even after incorporating decomposition rates into BEMF calculations for global forest ecosystems, tropical forests still exhibit considerably lower BEMF than polar/continental forests (Fig. S7a–c). Therefore, considering our results and previous studies[12,26], we conclude that soil nutrient pools, rather than belowground productivity or decomposition, are the primary drivers of observed high BEMF in Arctic ecosystems. Furthermore, observational studies consistently show that low water availability and nutrient pools limit belowground productivity and soil functions in dry biomes[24], thereby accounting for the lower BEMF observed in our study.

An abrupt shift in global belowground ecosystem multifunctionality was found along temperature

We investigated the coefficient of determination between BEMF and MAT, the coefficient is greater than the equivalent for MAP in temperate, dry, continental, and polar biomes, while an opposite result is observed in tropical biomes (Fig. 2a). Globally, our results confirm that temperature ($R^2 = -0.59$, $p < 0.01$), rather than precipitation ($R^2 = 0.01$, $p < 0.01$), is the key factor affecting BEMF (Fig. 2a). Subsequent application of piecewise linear regression fitting identifies an abrupt shift in global BEMF at a MAT threshold of 16.4 °C (Fig. 2b). Two distinct BEMF patterns are identified: high BEMF (HBEMF, mean value = 0.43; $BEMF = 0.43 - 0.0130*MAT$, $p < 0.0001$) and low BEMF (LBEMF, mean value = 0.21; $BEMF = 0.25 - 0.0017*MAT$, $p < 0.0001$). Globally, in regions with MAT ≤ 16.4 °C (HBEMF pattern), BEMF rapidly decreases with increasing temperature, while in regions with MAT > 16.4 °C (LBEMF pattern), the effect of temperature on BEMF is negligible (Fig. 2b). Actually, many investigations reveal ecosystem structure varying with climatic elements, including temperature (i.e., fungal decomposers and respiration)[27,28] and aridity (i.e., plant diversity and ecosystem productivity)[2,6,29,30]. Our results reinforce the contention, based thus far on only a limited range of ecosystems and regions (i.e., drylands, Tibetan Plateau, and north China[1,2,7]), that ecosystem multifunctionality globally is characterized by thresholds in climate.

The driving factors of belowground ecosystem multifunctionality

To identify the driving factors of the observed spatial BEMF patterns, we performed linear regression analysis using seven factors: MAT and MAP (Fig. S4), plant species richness and soil biodiversity (Fig. S5), and soil pH, bulk density, and clay content (Fig. S6). As evident in Fig. 2d, in regions with MAT > 16.4 °C (LBEMF pattern), BEMF is correlated with several factors, including MAP, soil pH, clay, bulk density, plant species richness, and soil biodiversity. Structural equation modeling analysis (SEM) further confirms that precipitation dominates the dynamics of BEMF via its effects on biodiversity and soil physical properties (Fig. 3b), even after accounting for the simultaneous direct and indirect effects of these indicators (Figs. S8b and S9b).

In the LBEMF pattern (MAT > 16.4 °C), low water availability in dry biomes limits ecosystem functioning and soil fertility. Many plant and soil organisms in drylands struggle to thrive under conditions of limited moisture and nutrients[9]. For example, sharp declines in soil carbon sink, soil taxa diversity, and soil nutrients occur when water

 https://doi.org/10.1038/s41467-025-64453-4

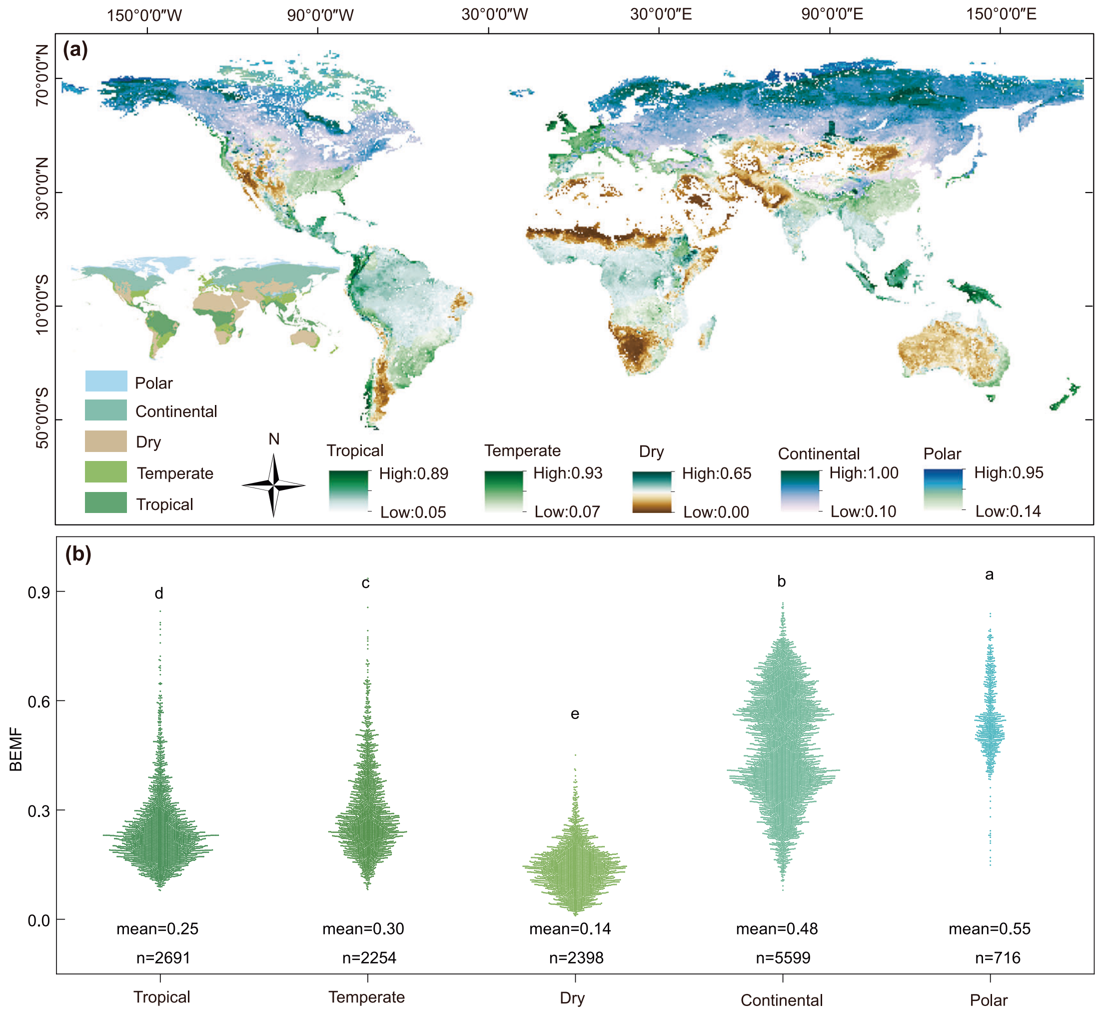

Fig. 1 | BEMF at the global scale. a Global map of BEMF. **b** BEMF varies across Köppen climate biomes; significant differences are denoted by different letters ($p < 0.05$). The numbers of n represent the number of data entries in the corresponding region. The significance level was evaluated using a two-sided t-test. BEMF constitutes indicators that relate to ecosystem productivity (i.e., belowground biomass), nutrient pools and cycling (i.e., soil nutrients, mineralization, decomposition, respiration, etc.). BEMF belowground ecosystem multifunctionality.

availability falls below 25%[9]. Increased precipitation, observed across a gradient from dry (MAP = 296.0 mm) to tropical (MAP = 1694.9 mm) biomes (Fig. S10a), will increase soil water availability, further accelerating biogeochemical cycles and microbial decomposition in tropical biomes. Thus, decomposition rates are much higher in tropical than in dry biomes[22], and decomposition is a primary source of available inorganic nutrients (nitrogen and phosphorus) in tropical biomes, supporting higher biodiversity and ecosystem functions (belowground productivity and biological carbon sequestration)[9,31]. Moreover, plant species richness, strongly influenced by precipitation, is also a key driver of BEMF (as reflected by SEM, Fig. 3b). Higher plant species richness in tropical biomes (36.36) compared to dry biomes (10.62, Fig. S10b) benefits multiple ecosystem functions related to productivity and nutrient cycling [29,32]. Indeed, it has been well-demonstrated that precipitation and high plant species richness positively shape ecosystem functions via their effects on ecosystem stability, resource acquisition, productivity, and plant–microbe interactions[5,9,30].

In contrast, in the HBEMF pattern (MAT ≤ 16.4 °C), biodiversity exhibits a weak relationship with BEMF (Fig. 2a). Low temperatures (MAT = −0.91 °C, Fig. S12a) act as an environmental filter in HBEMF regions, selecting species with specific climate niches. As highlighted in previous studies[10,32], biodiversity remains relatively consistent from 40°N to 80°N (Fig. S5), which results in limited impacts on BEMF. Furthermore, the influence of biodiversity on ecosystem functions varies across biomes, manifesting as positive, neutral, or negative effects. This variation arises because the response of multifunctionality to biodiversity can be regulated by various confounding factors, such as abiotic properties[8,33], plant functional traits[6], and the number of functions[34]. Thus, it is essential for future research to prioritize unraveling how biodiversity is associated with ecosystem multifunctionality in some contexts while not in others[34–36].

Furthermore, in the HBEMF pattern, temperature and soil pH generate strong negative effects on BEMF (Figs. 3a, S8a, and S9a). In cold ecosystems, soil functions linked to microorganisms are extremely sensitive to temperature and pH variations[37]. Increasing temperature from polar (MAT = −12.4 °C) to continental biomes (MAT = −2.0 °C, Fig. S11a) enhances soil microbial respiration, releasing carbon and reducing soil functions. Elevated temperature from polar to dry biomes (MAT = 8.2 °C, Fig. S11a), coupled with water deficits (MAP = 213.9 mm, Fig. S11b), intensifies water stress in dry biomes, and further suppresses ecosystem processes and degrades multiple functions[1,2,9]. For example, high temperatures (or extreme drought) in drylands reduce the capacity for multiple functions related to carbon, nitrogen, and phosphorus cycling[5] and potentially reduce plant species richness[38], negatively impacting ecosystem functions. This mechanism is supported by the SEM (Fig. 3a), confirming a strong negative effect of temperature on BEMF. Moreover, our findings align

https://doi.org/10.1038/s41467-025-64453-4

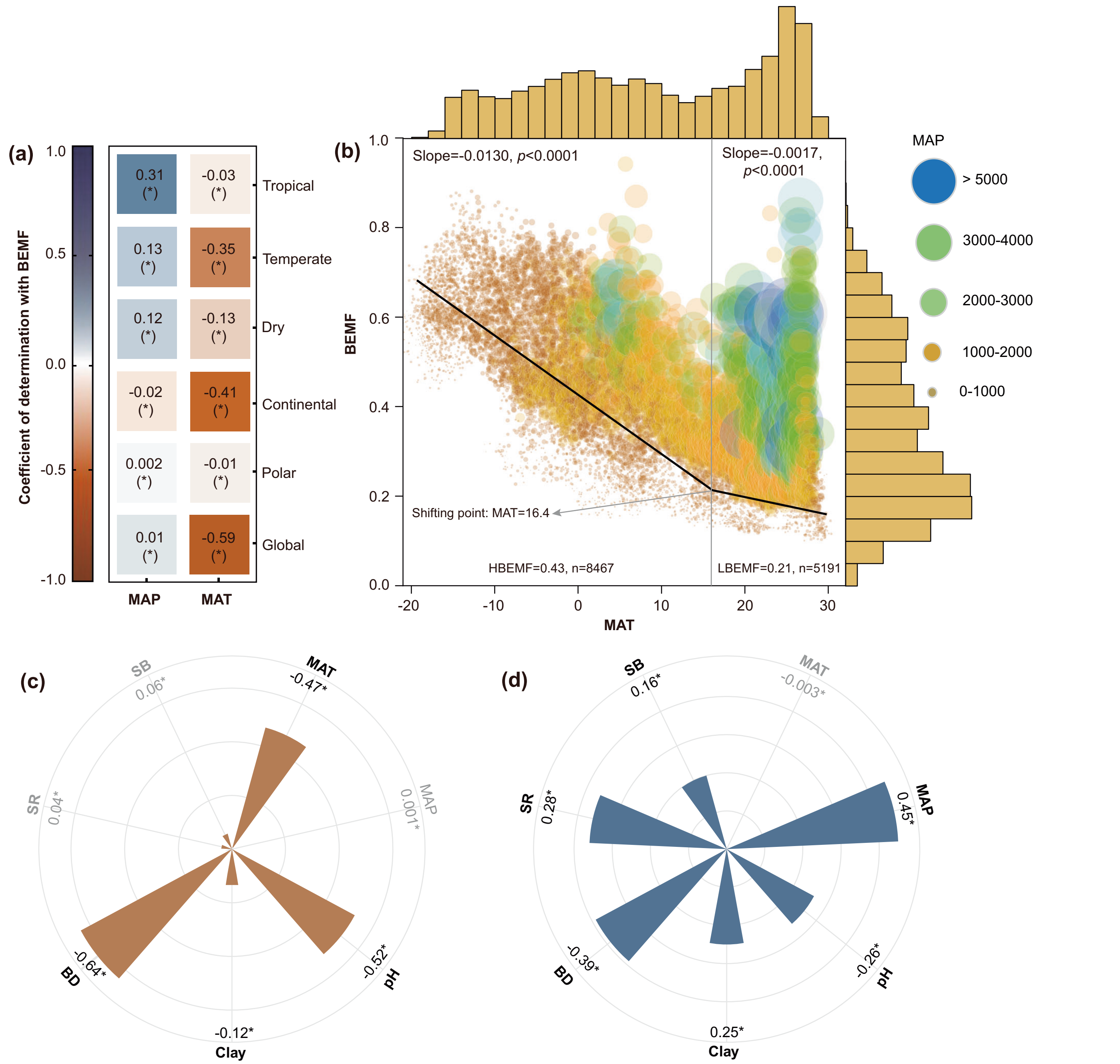

Fig. 2 | Relationships between environmental factors and BEMF. a Coefficient of determination (R^2) between MAP (mm) and BEMF, MAT (°C) and BEMF in Köppen climate biomes and globally. **b** Piecewise linear regression fitting identifies the threshold of MAT where global BEMF shifts abruptly. When MAT ≤ 16.4 °C, BEMF = 0.43−0.0130*MAT ($p < 0.0001$); when MAT > 16.4 °C, BEMF = 0.25−0.0017*MAT ($p < 0.0001$). Both the size and color of the circles represent the MAP. Coefficient of determination (R^2) between BEMF and environmental factors in regions with high BEMF (HBEMF, **c**) and low BEMF (LBEMF, **d**). *Note*: if the coefficient of determination between the environmental factors and BEMF is > 0.1 (factors in black fonts), the factor can be considered an important determinant affecting BEMF and further used in structural equation modeling (SEM). In other words, the factors in grey fonts are not used in the following SEM. "–" Represents that there is a negative relationship. * Indicates that the relationship is statistically significant at $p < 0.01$. BEMF belowground ecosystem multifunctionality, MAT mean annual temperature, MAP mean annual precipitation, SR plant species richness, SB soil biodiversity, BD soil bulk density.

with the observation that soil pH is typically acidic in continental ecosystems (pH = 5.99, due to organic matter accumulation) but more alkaline in dry biomes (pH = 7.81, Fig. S11c). Temperature and soil pH are often synchronized[4,8] as soil $CaCO_3$ dissolves more readily at higher temperatures[5,9]. Alkaline soils in dry biomes are less supportive of plant survival and growth[8], making pH a key driver of BEMF through its negative effects on belowground productivity and nutrient cycling[1,4,39].

In summary, we found that temperature influences BEMF in regions with MAT ≤ 16.4 °C (high BEMF pattern, with average values of MAT = 0.2 °C and MAP = 522.9 mm), while precipitation dominates BEMF in regions where MAT > 16.4 °C (low BEMF pattern, with average values of MAT = 23.5 °C and MAP = 1161.9 mm, Fig. S12). These observed patterns may be partially explained by an additional hypothesis. The position of the 16.4 °C line closely aligns with the Tropic of Cancer (Fig. S13). As is well-known, the Tropic of Cancer is associated with the Earth's rotation and revolution, which shape distinct climates on either side of this latitude. The regions between the Tropic of Cancer and the Tropic of Capricorn are generally not limited

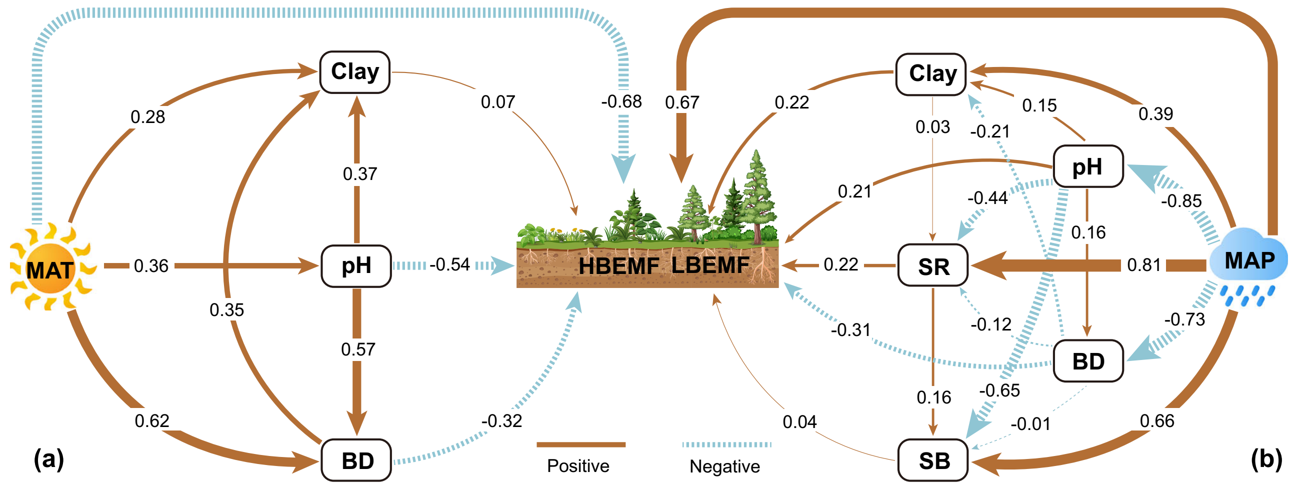

Fig. 3 | Standardized total effects of key environmental factors on BEMF. Structural equation modeling was conducted for two patterns of BEMF: regions with high BEMF (HBEMF, $R^2 = 0.76$, $X^2 = 3.1$, df = 1, $p = 0.08$, RMSEA = 0.00, **a**) and regions with low BEMF (LBEMF, $R^2 = 0.57$, $X^2 = 0.10$, df = 1, $p = 0.78$, RMSEA = 0.00, **b**). Orange and blue arrows indicate significant (if p-value $<$ 0.05, a two-sided test) positive and negative relationships (standardized path coefficients are rounded up to two decimal places), respectively. The width of each solid arrow is proportional to the standardized path coefficients. BEMF belowground ecosystem multifunctionality, MAT mean annual temperature, MAP mean annual precipitation, BD soil bulk density, SR plant species richness, SB soil biodiversity.

by heat due to high solar radiation. However, temperature remains the most critical limiting resource for organisms in cold ecosystems. Consequently, precipitation has a more significant influence on BEMF than temperature in the low BEMF pattern ($R^2 = 0.45$ vs. $R^2 = -0.003$, Fig. 2d). In contrast, temperature plays a more decisive role in shaping the BEMF than precipitation in the high BEMF pattern ($R^2 = -0.47$ vs. $R^2 = 0.001$, Fig. 2c).

Future belowground ecosystem multifunctionality

Results from both modeling and observational studies indicate that climate warming induces losses in both global biodiversity and permafrost soil carbon[13], thus raising the question of how BEMF may respond to ongoing climate change. This question is addressed by the results presented in Fig. 4, which illustrates the response of BEMF to different future climate scenarios (shared socioeconomic pathways, SSPs, SSP126, SSP370, and SSP585) for the years 2060 and 2100. Our results suggest that the simulated BEMF in biomes of temperate, continental, and polar regions is reduced by 14.3%, 32.9%, and 10.3% in 2100 (Fig. 4j–l), respectively, particularly in the Northern Hemisphere (Fig. 4a–f). Inversely, the simulated BEMF in the tropical and dry biomes is enhanced by 2.6% and 2.5% in 2100 (Fig. 4h, i), respectively, especially in South America, Africa, Indonesia, and Malaysia (Fig. 4a–f). Globally, a changing climate portends a 20.8% loss of BEMF in the SSP585 by 2100 (Fig. 4g).

These results highlight that global BEMF will be lost rapidly under ongoing warming, particularly in cold ecosystems of the Northern Hemisphere (Fig. 4). Several possible causes for this phenomenon are suggested as follows. (i) In the future, polar and continental ecosystems will experience remarkably rapid temperature increases (Fig. S14d, e), which are expected to accelerate the breakdown and release of carbon through microbial respiration[13,40]. For example, climate warming has already resulted in substantial soil carbon loss in high-latitude peatlands[12,13], particularly in Siberia and Alaska[14]. These northern peatlands store many of the global soil carbon stock[40], and any decrease in soil carbon associated with climate warming can have marked adverse effects on both regional and global ecosystem function[14]. (ii) Widespread and abrupt permafrost melting, along with the expansion of thermokarst lakes in the northern circumpolar permafrost, is already underway[13]. The resulting ground collapse exposes significant quantities of carbon that were previously frozen in anoxic and acidic environments to decomposition[13,20]. Modeling suggests that permafrost thawing in the Arctic could release between 60 billion and 100 billion tons of carbon into the atmosphere by 2300[19]. (iii) The increase in the frequency and magnitude of wildfires due to climate warming has already led to significant losses in timber-producing forests, particularly in the western USA and Canada[41]. This increased frequency and extent of wildfires may result in widespread degeneration of tundra and boreal forests, along with a loss of carbon stocks[40,42,43]. For example, in northern peatlands, climate warming is expected to amplify burn rate, significantly reducing the carbon sink by 65% by the year 2100[40]. (iv) Although rising temperatures are expected to promote decomposition and nutrient cycling functions in cold ecosystems[44], the elevated ecosystem respiration, loss of biodiversity, and permafrost carbon release due to warming may play a more significant role in the decline of belowground functions, leading to outputs exceeding inputs[19,45,46]. (v) There is an optimal temperature range for various ecosystem functions, including productivity[47], soil decomposition[27], and nutrient availability[48]. Exceeding this optimal range through future temperature increases may result in ecosystem degradation, potentially causing soil taxa mortality and reduced multifunctionality[2,9,27]. Taken together, under any (or all) of these mechanisms, climate warming in cold ecosystems may lead to a major loss of ecosystem multifunctionality.

Because the productivity of rainforests is limited by soil nutrients[23] related to vigorous leaching[49], the reduced precipitation in the tropical biomes (Fig. S15a) will likely promote tropical ecosystem functions in the future by reducing soil erosion and nutrient loss, and ultimately promote the nutrient pools in ecosystems. For example, meta-analysis has demonstrated that reduced precipitation has significantly increased nitrogen storage (12.0%) in humid regions[50]. Moreover, the decrease in future precipitation (Fig. S15a) and increase in future temperature (Fig. S14a) may exacerbate the frequency and intensity of droughts and heatwaves, further suppressing plant growth[51,52]. As a result, more tropical soil functions may be delayed. Conversely, in dry biomes, increased future precipitation (Fig. S15b) may enhance biocrust development, creating better habitats for microorganisms and potentially buffering the negative effects of extreme drought and dust on plants[39,53], potentially invoking a positive feedback loop, sustaining carbon sequestration[54] and microbial beta-diversity[55]. Increased biological richness may improve ecosystem resistance to extreme weather and desertification[5], enhancing ecosystem functions in dry biomes.

https://doi.org/10.1038/s41467-025-64453-4

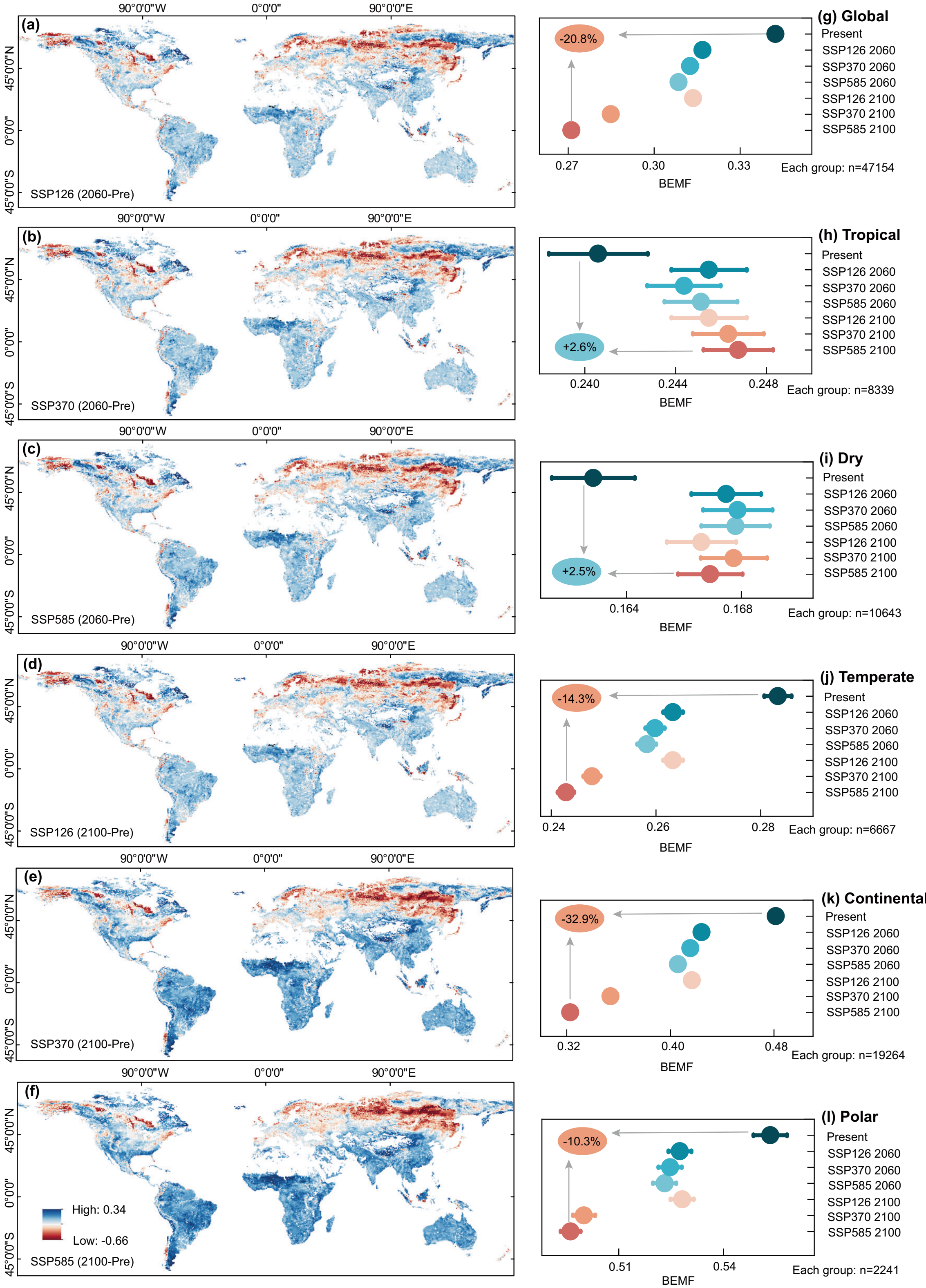

Fig. 4 | Future projections of BEMF. Change in BEMF between the present and 2060 in SSP126 (**a**), SSP370 (**b**), and SSP585 (**c**), respectively; and change of BEMF between the present and 2100 in SSP126 (**d**), SSP370 (**e**), and SSP585 (**f**), respectively. Current BEMF versus future BEMF for globally (**g**), and for tropical (**h**), dry (**i**), temperate (**j**), continental (**k**), and polar (**l**) biomes, respectively. The numbers in the red and blue ovals represent the decrease and increase rates of BEMF between the current and 2100 in SSP585, respectively. The numbers of *n* represent the number of data entries in the corresponding region. Box plots display means (solid dots), and whiskers represent the 95% confidence interval. BEMF belowground ecosystem multifunctionality, SSP shared socioeconomic pathways, Pre present.

https://doi.org/10.1038/s41467-025-64453-4

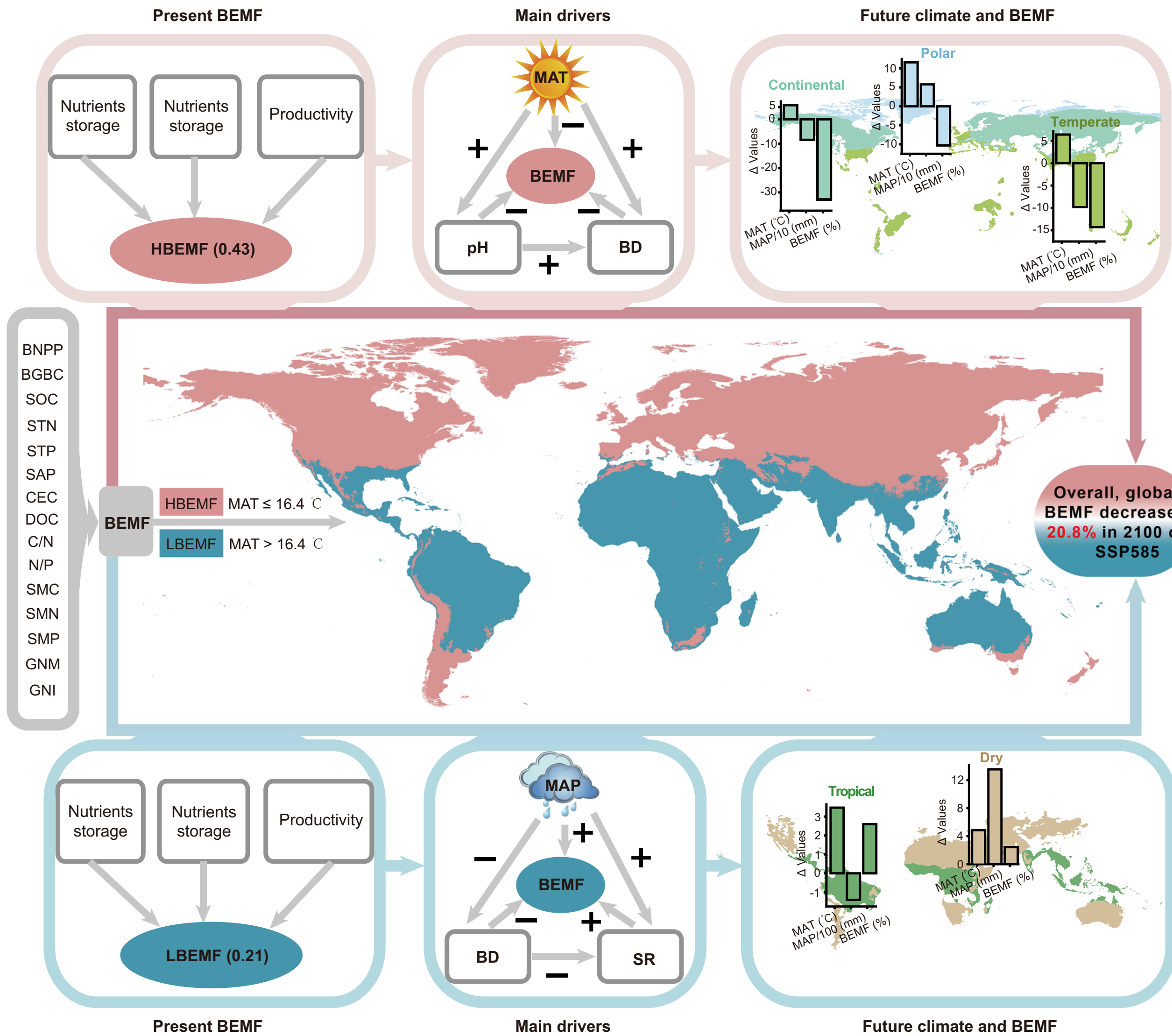

Fig. 5 | Global distribution, control mechanisms, and future dynamics of BEMF. Fifteen indicators for key ecosystem functions were used to calculate global BEMF. MAT abruptly shifts BEMF at a threshold of 16.4 °C. When MAT ≤ 16.4 °C, high BEMF (0.43) is driven by MAT mainly through its effect on soil pH and BD. In contrast, when MAT > 16.4 °C, low BEMF (0.21) is mainly determined by MAP through its effects on soil BD and SR. The variation of climate and BEMF between the present and future (2100 in SSP585) is shown in different biomes and globally. Ecosystem function dataset: BNPP belowground net primary productivity, BGBC belowground living biomass carbon stock density, SOC soil organic carbon, STN soil total nitrogen, STP soil total phosphorus, SAP soil available phosphorus, CEC cation exchange capacity, DOC soil dissolved organic carbon, C/N SOC/STN, N/P STN/STP, SMC soil microbial carbon, SMN soil microbial nitrogen, SMP soil microbial phosphorus, GNM gross nitrogen mineralization rate, GNI gross nitrogen immobilization rate, MAT mean annual temperature, MAP mean annual precipitation, BEMF belowground ecosystem multifunctionality, SR plant species richness, BD soil bulk density, LBEMF low BEMF, HBEMF high BEMF.

Limitations and implications of the current study

Despite extensive research over recent decades indicating that ecosystem multifunctionality is driven by climate through its effects on biodiversity, much of this work has largely focused on regional grassland ecosystems, such as those in northern China[1] and the Tibetan Plateau[7], or has been limited to specific environmental conditions, like global drylands[5]. Moreover, many previous studies primarily addressed the relationship between ecosystem multifunctionality and the current climate index of aridity[1,6]. Consequently, there remains a gap in understanding the global pattern and response of ecosystem multifunctionality to future climate change. Our study addresses this knowledge gap by providing evidence of the relationship between climate and global BEMF, offering significant insights into the contrasting impacts of temperature and precipitation on BEMF at the threshold of MAT = 16.4 °C. Importantly, our findings highlight that climate change is expected to have negative consequences on BEMF by 2100, especially in cold ecosystems such as continental and polar biomes (Fig. 5). This underscores the need for climate-specific conservation strategies aimed at preserving ecosystem functions in these vulnerable regions.

While the indicators of soil-mediated nutrient pools (soil organic carbon, total nitrogen, and total phosphorus) are not direct measures of ecosystem functions (energy and matter fluxes), they are known to be critical determinants of ecosystem function and biodiversity[1,6,8,39] and to reflect long-term nutrient balance[21,56]. However, inconsistencies in the dataset's timelines, depth, and spatial resolution may introduce errors in BEMF calculations. Therefore, future studies should include further parameters related to ecosystem energy and matter fluxes (e.g., basal respiration, decomposition, nutrient leaching, etc.)[31,57], rather than inactive carbon stocks. Indeed, as indicated by the previous references in Table S1, there is no consensus regarding which indicators should be considered appropriate for assessing ecosystem functions. To advance future BEMF research, greater attention must be devoted to the selection, measurement, and interpretation of ecosystem functions. For further insights into the process of selecting indicators that relate to ecosystem functions, we recommend consulting the review study[56]. Additionally, beyond the seven environmental factors considered in our study, other biological and abiotic factors—such as land-use change, grazing, nitrogen deposition, invasions, in situ soil biodiversity, and phylogenetic richness—should also be incorporated[31,58,59]. Finally, another limitation of our study is estimating future BEMF with the Random Forest model rather than ecosystem process models, given the unavailability of many environmental factors associated with ecosystem functions globally[58]. Despite this constraint, our global simulation of BEMF provides valuable insights into the scientific conservation of ecosystem functions in hotspots (e.g., continental and polar biomes). To reduce uncertainties in simulating ecosystem multifunctionality, integrating long-term plot-level monitoring data into prediction models is essential. Our study calls for a broader understanding of BEMF-climate relationships across biomes, especially within the context of climate change.

In summary, our study provides evidence that temperature induces abrupt shifts in global BEMF at a threshold of 16.4 °C. Our analysis further suggests that temperature and precipitation drive BEMF in cold and tropical ecosystems, respectively. Notably, the release of permafrost carbon into the atmosphere under a warm climate may lead to a rapid reduction in BEMF by 2100, particularly in the Northern Hemisphere. An improved understanding of the interaction between BEMF and climate at the global scale is critical to take action to mitigate the negative effects of climate change for ecosystem sustainability and human well-being.

Methods

Ecosystem function data

The following criteria were used to select ecosystem data for this study: (a) Ecosystem indicators must be linked to key ecosystem processes and functions (e.g., belowground productivity, biological carbon sequestration, nutrient pools, and fluxes). (b) As indicated in Table S1, the indicators should have been used in prior multifunctionality studies. (c) Indicators must be publicly available as global raster data, apart from gross nitrogen mineralization and immobilization rates, which are sourced from a database developed by our team. The decomposition rate was excluded from our analysis as data were only available for global forests; however, we utilized the global forest decomposition rate to update the BEMF index and assess its distribution across Köppen climate biomes, as detailed in Fig. S7. (d) To minimize resampling errors, raster data resolution was limited to no more than 0.5°. Additionally, soil depth was restricted to a maximum of 50 cm, as topsoil properties are more susceptible to climatic and biological influences. Ultimately, we used fifteen ecosystem indicators (Table S2) related to key ecosystem functions to evaluate global BEMF.

Belowground net primary productivity. Belowground net primary productivity is an important ecosystem function that influences the carbon cycle by linking atmospheric CO_2 and soil carbon reservoirs. In our study, belowground net primary productivity (sequential soil depths down to 2 m) was downloaded from the figshare with a resolution of 1 km[60].

Belowground biomass carbon. The belowground living biomass carbon stock density acts as an appropriate indicator of biological productivity[61]. Data for this parameter relating to the carbon stock in living roots of woody and herbaceous cover was sourced from ORNL DAAC at a resolution of 300 m for the year 2010. Belowground living biomass carbon stock density includes carbon stored in living plant tissues located below the earth's surface (roots). This does not include dead and/or dislocated root tissue, nor does it include soil organic matter[61].

Soil nutrient pools and fluxes. Data for soil (0–5 cm depth) cation exchange capacity, soil organic carbon, and soil total nitrogen at a spatial resolution of 250 m was obtained from the SoilGrids data set[62], soil total phosphorus (0–10 cm depth)[63] at a spatial resolution of 0.5° and soil available phosphorus (0–20 cm depth)[64] at a spatial resolution of 1 km were downloaded from the figshare. Meanwhile, we calculated the ratios of soil organic carbon/total nitrogen and soil total nitrogen/total phosphorus, because these ratios are important indices to measure soil fertility.

Soil dissolved organic carbon is a primary form of labile carbon in terrestrial ecosystems, which plays a vital role in soil carbon cycling[65]. Soil dissolved organic carbon (0–30 cm depth) was obtained from the Dryad with a spatial resolution of 0.5°.

The dynamics of organic decomposition microbial activity, as indicated by microbial biomass[66], was freely available from the Compilation of Global Soil Microbial Biomass Carbon, Nitrogen, and Phosphorus. Data at a spatial resolution of 0.5° (0–30 cm)[66].

The gross nitrogen mineralization rate is a key process within the nitrogen cycle, transforming organic nitrogen into inorganic nitrogen. Gross nitrogen immobilization rate is an important nitrogen source for both microorganisms and plants[4]. These indicators serve as effective proxies for the processes driving nutrient fluxes. The global distribution of the gross nitrogen mineralization rate used in this paper is derived from the sum of soil mineralization rates and litter mineralization rates from previous studies[67,68]. Additionally, the global distribution of gross microbial nitrogen immobilization rates used in this study is sourced from another previous investigation[69].

Finally, fifteen ecosystem function datasets described above are used as a proxy for ecosystem function linked to productivity, soil fertility, nutrient fluxes, and composition of carbon pools[1]. These databases were resampled to 0.5° resolution using ArcMap 10.8 (Environmental Systems Research Institute, Inc., Redlands, CA, USA) and then used to calculate the global BEMF. Next, we applied three basic approaches (the average method, the principal component method, and the single threshold method, see "Data analyses" subsection in the "Methods" section) to explore the spatial patterns of BEMF values.

Environmental factors

Climate data. Given that climate is closely related to ecosystem functions[1,9], historical bioclimatic data (1970–2000) of data (precipitation and temperature) at a spatial resolution of 10′ were downloaded from WorldClim[70] and used to evaluate the relationship between climate and BEMF.

Soil abiotic data. Previous studies have shown that soil physical properties influence ecosystem multifunctionality[1,4,8]. Accordingly, soil physical properties (0–5 cm depth), specifically soil pH, percentage clay (<0.002 mm), and bulk density, were retrieved from the SoilGrids dataset, with a 250 m spatial resolution.

Biodiversity data. Biodiversity plays a vital role in regulating multiple ecosystem functions[3,8]. The distribution of soil biodiversity, illustrating the potential diversity of living organisms in soils (i.e., microorganisms, fauna, and biological functions) globally at a spatial resolution of 0.1°, was acquired from the European Soil Data Centre (ESDAC)[71].

Global native vascular plant species richness data at a spatial resolution of 0.05° were obtained from the Anthroecology Lab[72]. The number of native vascular plant species is estimated by the species richness model that is based on empirical statistical relationships between environment and species richness obtained from datasets documenting the number of aboveground native species in 1032 geographic regions worldwide.

https://doi.org/10.1038/s41467-025-64453-4

All environmental factors (climate data, soil abiotic data, and biodiversity data) were resampled to 0.5° using ArcMap 10.8, to evaluate their relationships with BEMF further.

Köppen–Geiger climate classification data

We used the Köppen–Geiger climate classification to discern whether there is a discrepancy of BEMF in different climate biomes. The global maps of the Köppen–Geiger climate classification were downloaded from figshare with a resolution of 1 km[73]. The Köppen climate classification is a system based on the regional temperature and precipitation. In detail, the tropics are warm and humid (MAT = 24.76 °C, MAP = 1689.67 mm), but the continental (MAT = −2.0 °C, MAP = 499.43 mm) and polar (MAT = −12.39 °C, MAP = 260.45 mm) biomes are relatively cold, and the dry biomes are dry (MAT = 18.30 °C, MAP = 267.13 mm).

Assessment of BEMF

The averaging, PCA, and single-threshold approaches were used to calculate the global maps of BEMF using ArcGIS Pro 3.1.5. The averaging approach has been consistently applied in previous research[74]. To ensure all ecosystem function data are in the same dimension, all ecosystem function data should be standardized before calculating. There are mainly two standardization methods of ecosystem function, namely, the *Z*-score method and the conversion method of maximum value. In our study, we calculated the standardized values using the *Z*-scores as described in the previous ref. 75, and the averaging approach collates the mean values of each standardized function in each 0.5° grid. The average approach is calculated as follows:

$$\mathrm{BEMF}_{\mathrm{average}} = \frac{1}{F}\sum_{i=1}^{F} g(r_i(f_i)) \tag{1}$$

where F represents the number of ecosystem functions; f_i is the value of ecosystem function in ith; r_i is a mathematical function that converts values to positive; g is a standardized treatment.

Compared to the averaging approach, the advantage of the PCA method is that it can reduce dimensions, prevent collinearity between indicators, and retain the information of each indicator[76]. Applying PCA does not involve the multiple contributions of correlated ecosystem functions[77]; the principal component axis in multifunctional space is calculated for fifteen standardized functions for each grid square. We then summed the PCA axis scores weighted by the degree of contribution of each axis into a single index to quantify BEMF. The PCA calculation method is as follows:

$$\mathrm{BEMF}_{\mathrm{PCA}} = \sum_{i=1}^{n} a_i \mathrm{PC}_i \tag{2}$$

where PC_i is the ith principal component; α_i is the contribution rate corresponding to the ith principal component; n is the total number of principal components selected. The first two principal components were used in our study, so n is equal to 2.

There is unprecedented heterogeneity of thresholds in each grid spanning a global scale that will lead to the calculation of global BEMF inapplicably using the multiple-threshold approach based on the ecosystem functions without time series; thus, we utilized the recommended method (the single-threshold) as described in the previous ref. 78. We employed the single-threshold to quantify BEMF and selected the 50% maximum for each ecosystem function as the threshold following the next two reasons: (1) If an ecosystem can provide 50% of the maximum species for a function, thereby considering that the ecosystem can maintain this function by referencing the median lethal effect concentration in ecotoxicology; (2) For any single function, on average one species was needed to maintain a specific process at ~60% of the maximum rate. Thus, selecting 50% as the threshold can maximize the probability, i.e., one function at least needs a species to sustain. It is important to note that the maximum represents the range at the top 5% of each ecosystem function, and that is to prevent outliers. After determining the threshold and maximum, we counted the total number of ecosystem functions that passed the prescribed threshold and thereby produced the global map of BEMF with the threshold approach. The single-threshold calculation method is as follows:

$$\mathrm{BEMF}_{\mathrm{threshold}} = \sum_{i=1}^{F}\sum_{j=1}^{k}\left(r_{ij}(f_{ij}) > t_i\right. \tag{3}$$

where F is the number of ecosystem functions; k is the total number of grid pixels of the ecosystem function. f_{ij} is the jth value of the ith ecosystem function; r_{ij} is a mathematical function that converts values to positive; t_i is the ith ecosystem function threshold.

Although we used three basic approaches to assess worldwide BEMF, each approach has merits and demerits (Table S3)[79,80]. To address this issue, we averaged the three indexes after normalization to synthetically represent BEMF.

Similarity analysis of BEMF

We used two methods to examine the spatial similarity of BEMF using different approaches. To compare the similarity of BEMF, the comparison map profile (CMP) method was used, which employs the averaged values of cross-correlation coefficient (CC) and absolute distance (DD) from scales 1 (3 × 3 pixel moving window) to 10 (30 × 30 pixel moving window), their computational formula as follows[81]:

$$\mathrm{DD} = abs(\bar{x} - \bar{y}) \tag{4}$$

$$\mathrm{CC} = \frac{1}{N^2}\sum_{i=1}^{N}\sum_{j=1}^{N}\frac{(x_{ij}-\bar{x})(y_{ij}-\bar{y})}{\sigma_x\sigma_y} \tag{5}$$

$$\sigma_x^2 = \frac{1}{N^2-1}\sum_{i=1}^{N}\sum_{j=1}^{N}(x_{ij}-\bar{x})^2 \tag{6}$$

where $\bar{x}$ and $\bar{y}$ denote the averaged values of two moving windows for the two comparative images. x_{ij} and y_{ij} represent pixel values of two moving windows in two compared images in row i and column j, respectively. σ_x and σ_y denote the standard deviation corresponding to two moving windows of two comparative images. N is the pixel number of moving windows. Low DD and high CC values indicate more substantial similarity between two images, and vice versa. In addition, we used the Taylor Diagram and comparison map profile (CMP) to compare the similarity of BEMF based on the different approaches. This method is performed by the R 4.1.1 software (R Core Development Team, R Foundation for Statistical Computing, Vienna, Austria) using the "*openair*" package.

Global spatial patterns based on the three BEMF approaches (averaging, PCA, and single-threshold) are consistent (Fig. S16a–c), as shown by Taylor diagrams (all $r > 0.75$, standard deviation < 0.20, and RMS error < 0.15; Fig. S17). Concordance correlation coefficient (CC) and discrepancy (DD) values indicate strong agreement between the averaging and PCA approaches (geometric mean CC = 0.64, geometric mean DD = 0.06; Fig. S18a, g), supporting the robustness of the PCA approach. Similarly, the averaging and threshold approaches show a strong correlation (geometric mean CC = 0.83, geometric mean DD = 0.06; Fig. S18b, h). However, the PCA and threshold approaches exhibit lower consistency (geometric mean CC = 0.31, geometric mean DD = 0.11; Fig. S18c, i), likely due to the discrete nature of the threshold approach. To address this discrepancy, we calculated the mean BEMF using the three approaches. This improves consistency between approaches in most areas (averaging-mean: geometric mean CC = 0.88, geometric mean DD = 0.06, Fig. S18d, j; PCA-mean: geometric mean CC = 0.52, geometric mean DD = 0.10, Fig. S18e, k; threshold-mean: geometric mean CC = 0.59, geometric mean DD = 0.10, Fig. S18f, l).

Data analyses

To eliminate the effects of differences in computing scale, we used log transformations to normalize the BEMF produced by the averaging, PCA, and single-threshold approaches. We averaged the BEMF calculated by the above three methods and further analyzed the BEMF through the following steps. Firstly, to explore the differences in BEMF between Köppen climate biomes (tropical, temperate, dry, continental, and polar), one-way ANOVAs with the Least Significant Difference (LSD) multiple comparisons were applied in R 4.1.1 software. Then, linear regression analysis was performed in SigmaPlot 10.0 (Systat Software, Inc., Chicago, IL, USA) to investigate relationships (R^2) between the BEMF and climate (precipitation and temperature) across the Köppen climate biomes and globally, the computational formula as follows:

$$Y = aX + Y_0 \tag{7}$$

where Y is the dependent variable of BEMF; α is the coefficient between variables of Y and X; X represents the climate of precipitation or temperature; Y_0 is a constant.

Secondly, given the strong correlation between temperature and BEMF at the global scale (Fig. 2a), piecewise linear regression fitting was conducted in SigmaPlot 10.0 to identify the existence of any thresholds, the computational formula as follows:

$$y = \begin{cases} \frac{y_1(T_1-t)+y_2(t-t_1)}{T_1-t_1}, t_1 \le t \le tT_1 \\ \frac{y_2(t_2-t)+y_3(t-T_1)}{t_2-T_1}, T_1 \le t \le t_2 \end{cases} \tag{8}$$

where y represents BEMF; t represents the climate of temperature; t_1 is the minimum value of t; t_2 is the maximum value of t; T_1 repesents the threshold of MAT in our study; y_1, y_2, and y_3 are the values of BEMF that corresponding to t_1, T_1, and t_2, respectively.

Indeed, an abrupt change of BEMF was detected using this method at a MAT threshold of ~16.4 °C (Fig. 2b), and this figure was plotted using Origin 2024 (Origin Ro, Version 2024. OriginLab Corporation, Northampton, MA, USA). We then used linear regression analysis to evaluate the relationships between environmental factors of climate (MAT, and MAP), soil physical properties (pH, clay, and bulk density), as well as biodiversity properties (soil biodiversity, and plant species richness) and BEMF (Fig. 2 c, d), and plotted these figures by R 4.1.1 software with the packages of "*ggplot2*" and "*gridExtra*". Meanwhile, if the absolute value of the coefficient of determination between the environmental factors and BEMF is >0.1, the factor can be considered an important determinant affecting BEMF, and further used in the SEM.

Thirdly, SEM was used to elucidate the direct and indirect relationships between BEMF, climate, soil properties, and biodiversity. An a priori structural equation modeling, based on previous studies[1,4,7,8], hypothesized causal relationships among these factors (Fig. S19). Before modeling, correlations between BEMF and its indicators were assessed to identify key influential factors. The model was parameterized using the selected dataset in AMOS 21.0 (Amos Development Corporation, Chicago, IL, USA). Model fit was evaluated using the root mean square error of approximation (RMSEA; acceptable fit: $0.00 \le \text{RMSEA} \le 0.05$), chi-squared test ($\chi^2$), and probability level (p; acceptable fit: $p > 0.05$)[8].

Next, we assume that other factors (e.g., land-use, soil properties, and biodiversity) remain unchanged in the future to isolate the impact of climate change on BEMF. Our SEM results provide convincing evidence that temperature and precipitation primarily control BEMF in high and low BEMF patterns, respectively. Based on previous studies[82–85], to screen machine learning models with high accuracy for simulating BEMF, four models (Random Forest, Boosted Regression Trees, Support Vector Machine, and Gradient Boosting Machine) were used in our study. We found that the Random Forest model exhibited high robustness and accuracy for predicting BEMF across both MAT ≤ 16.4 °C (high BEMF) and MAT > 16.4 °C (low BEMF) regions (Table S4). Consequently, we utilized the Random Forest model to simulate future BEMF changes under climate change scenarios. In detail, in both temperature-regulated and precipitation-regulated regions, the Random Forest algorithm was deployed to estimate BEMF and map its spatial patterns under three different future climate scenarios. SSP126 represents the sustainable development and low-emission pathway, SSP370 represents the imbalance development and intermediate emission pathway, and SSP585 represents the rapid development and high emission pathway[86]. Future bioclimatic data (MAT, mean diurnal range, isothermality, temperature seasonality, max temperature of warmest month, min temperature of coldest month, temperature annual range, mean temperature of wettest quarter, mean temperature of driest quarter, mean temperature of warmest quarter, and mean temperature of coldest quarter, MAP, precipitation of wettest month, precipitation of driest month, precipitation seasonality, precipitation of wettest quarter, precipitation of driest quarter, precipitation of warmest quarter, precipitation of coldest quarter) were obtained from the following ten models: ACCESS-CM2, CMCC-ESM2, EC-Earth3-Veg, GISS-E2-1-G, INM-CM5-0, IPSL-CM6A-LR, MIROC6, MPI-ESM1-2-HR, MRI-ESM2-0, and UKESM1-0-LL. In both temperature- and precipitation-regulated regions, the future bioclimatic data were divided into training (70%) and testing (30%) datasets. We configured the Random Forest regression model with 500 decision trees using the "*randomForest*" package in R software version 4.1.1. The model was then used to predict BEMF spatial patterns under the three different SSPs for two future periods (2021-2060 and 2061-2100). Model performance was evaluated using several metrics: correlation coefficient (CC), relative bias (BIAS), Nash–Sutcliffe coefficient efficiency (NSE), root mean square error (RMSE), and mean error (ME), calculated using test datasets. These metrics assessed the reliability of the predicted BEMF values. This comprehensive approach, leveraging extensive bioclimatic data and rigorous validation metrics, ensures the reliability and robustness of the Random Forest model in mapping BEMF under different climate scenarios.

Reporting summary

Further information on research design is available in the Nature Portfolio Reporting Summary linked to this article.

Data availability

The calculated belowground ecosystem multifunctionality (BEMF) and the predicted future BEMF generated in this study have been deposited in the Institute of Tibetan Plateau Research, Chinese Academy of Sciences, with open access (https://doi.org/10.11888/Terre.tpdc.301230). Detailed information for the ecosystem function data and environmental factors data used in this study is provided in the Supplementary Information (Table S2).

Code availability

The related data analyses and modeling were performed using R 4.1.1 and Python 3.1.5. The code is publicly available at https://doi.org/10.11888/Terre.tpdc.301230.

References

1. Hu, W. et al. Aridity-driven shift in biodiversity–soil multifunctionality relationships. *Nat. Commun.* **12**, 5350 (2021).
2. Berdugo, M. et al. Global ecosystem thresholds driven by aridity. *Science* **367**, 787–790 (2020).
3. Bardgett, R. D. & van der Putten, W. H. Belowground biodiversity and ecosystem functioning. *Nature* **515**, 505–511 (2014).
4. Delgado-Baquerizo, M. et al. Microbial diversity drives multifunctionality in terrestrial ecosystems. *Nat. Commun.* **7**, 10541 (2016).
5. Maestre, F. T. et al. Plant species richness and ecosystem multifunctionality in global drylands. *Science* **335**, 214–218 (2012).
6. Berdugo, M., Kefi, S., Soliveres, S. & Maestre, F. T. Plant spatial patterns identify alternative ecosystem multifunctionality states in global drylands. *Nat. Ecol. Evol.* **1**, 3 (2017).
7. Jing, X. et al. The links between ecosystem multifunctionality and above- and belowground biodiversity are mediated by climate. *Nat. Commun.* **6**, 8159 (2015).
8. Delgado-Baquerizo, M. et al. Multiple elements of soil biodiversity drive ecosystem functions across biomes. *Nat. Ecol. Evol.* **4**, 210–220 (2020).
9. Zhang, J. et al. Water availability creates global thresholds in multidimensional soil biodiversity and functions. *Nat. Ecol. Evol.* **7**, 1002–1011 (2023).
10. Gaston, K. J. Global patterns in biodiversity. *Nature* **405**, 220–227 (2000).
11. Greve, P. et al. Global assessment of trends in wetting and drying over land. *Nat. Geosci.* **7**, 716–721 (2014).
12. Plaza, C. et al. Direct observation of permafrost degradation and rapid soil carbon loss in tundra. *Nat. Geosci.* **12**, 627–631 (2019).
13. Schuur, E. A. et al. Climate change and the permafrost carbon feedback. *Nature* **520**, 171–179 (2015).
14. Wang, M. et al. Global soil profiles indicate depth-dependent soil carbon losses under a warmer climate. *Nat. Commun.* **13**, 5514 (2022).
15. Yang, Y. et al. Negative effects of multiple global change factors on soil microbial diversity. *Soil Biol. Biochem.* **156**, 108229 (2021).
16. Byrnes, J. et al. Multifunctionality does not imply that all functions are positively correlated. *Proc. Natl Acad. Sci. USA* **111**, E5490 (2014).
17. Constán-Nava, S., Soliveres, S., Torices, R., Serra, L. & Bonet, A. Direct and indirect effects of invasion by the alien tree *Ailanthus altissima* on riparian plant communities and ecosystem multifunctionality. *Biol. Invasions* **17**, 1095–1108 (2015).
18. Gherardi, L. A. & Sala, O. E. Global patterns and climatic controls of belowground net carbon fixation. *Proc. Natl Acad. Sci. USA* **117**, 20038–20043 (2020).
19. Turetsky, M. R. et al. Permafrost collapse is accelerating carbon release. *Nature* **569**, 32–34 (2019).
20. Fenner, N. & Freeman, C. Drought-induced carbon loss in peatlands. *Nat. Geosci.* **4**, 895–900 (2011).
21. Jing, X. et al. The influence of aboveground and belowground species composition on spatial turnover in nutrient pools in alpine grasslands. *Glob. Ecol. Biogeogr.* **31**, 486–500 (2022).
22. Seibold, S. et al. The contribution of insects to global forest deadwood decomposition. *Nature* **597**, 77 (2021).
23. Cunha, H. F. V. et al. Direct evidence for phosphorus limitation on Amazon forest productivity. *Nature* **608**, 558–562 (2022).
24. Du, E. Z. et al. Global patterns of terrestrial nitrogen and phosphorus limitation. *Nat. Geosci.* **13**, 221 (2020).
25. Hou, E. et al. Global meta-analysis shows pervasive phosphorus limitation of aboveground plant production in natural terrestrial ecosystems. *Nat. Commun.* **11**, https://doi.org/10.1038/s41467-020-14492-w (2020).
26. Rillig, M. C. et al. The role of multiple global change factors in driving soil functions and microbial biodiversity. *Science* **366**, 886–890 (2019).
27. Feng, Y. et al. Temperature thresholds drive the global distribution of soil fungal decomposers. *Glob. Change Biol.* **28**, 2779–2789 (2022).
28. Johnston, A. S. A. et al. Temperature thresholds of ecosystem respiration at a global scale. *Nat. Ecol. Evol.* **5**, 487–494 (2021).
29. Delgado-Baquerizo, M. et al. Soil microbial communities drive the resistance of ecosystem multifunctionality to global change in drylands across the globe. *Ecol. Lett.* **20**, 1295–1305 (2017).
30. Garcia-Palacios, P., Gross, N., Gaitan, J. & Maestre, F. T. Climate mediates the biodiversity–ecosystem stability relationship globally. *Proc. Natl Acad. Sci. USA* **115**, 8400–8405 (2018).
31. Luo, Y. H. et al. Multitrophic diversity and biotic associations influence subalpine forest ecosystem multifunctionality. *Ecology* **103**, e3745 (2022).
32. Kreft, H. & Jetz, W. Global patterns and determinants of vascular plant diversity. *Proc. Natl Acad. Sci. USA* **104**, 5925–5930 (2007).
33. van der Plas, F. Biodiversity and ecosystem functioning in naturally assembled communities. *Biol. Rev.* **94**, 1220–1245 (2019).
34. Gamfeldt, L. & Roger, F. Revisiting the biodiversity–ecosystem multifunctionality relationship. *Nat. Ecol. Evol.* **1**, 168 (2017).
35. Garcia, R. A., Cabeza, M., Rahbek, C. & Araujo, M. B. Multiple dimensions of climate change and their implications for biodiversity. *Science* **344**, 1247579 (2014).
36. Berlinches de Gea, A., Hautier, Y. & Geisen, S. Interactive effects of global change drivers as determinants of the link between soil biodiversity and ecosystem functioning. *Glob. Change Biol.* **29**, 296–307 (2023).
37. Davison, J. et al. Temperature and pH define the realised niche space of arbuscular mycorrhizal fungi. *N. Phytol.* **231**, 763–776 (2021).
38. Shi, H. et al. Terrestrial biodiversity threatened by increasing global aridity velocity under high-level warming. *Proc. Natl Acad. Sci. USA* **118**, https://doi.org/10.1073/pnas.2015552118 (2021).
39. Delgado-Baquerizo, M. et al. Biocrust-forming mosses mitigate the negative impacts of increasing aridity on ecosystem multifunctionality in drylands. *N. Phytol.* **209**, 1540–1552 (2016).
40. Wilkinson, S. L. et al. Wildfire and degradation accelerate northern peatland carbon release. *Nat. Clim. Change* **13**, 456–461 (2023).
41. Bousfield, C. G., Lindenmayer, D. B. & Edwards, D. P. Substantial and increasing global losses of timber-producing forest due to wildfires. *Nat. Geosci.* **16**, 1145–1150 (2023).
42. Liang, L., Liang, S. & Zeng, Z. Extreme climate sparks record boreal wildfires and carbon surge in 2023. *Innovation (Cambridge, MA)* **5**, 100631–100631 (2024).
43. Virkkala, A.-M. et al. Wildfires offset the increasing but spatially heterogeneous Arctic-boreal CO_2 uptake. *Nat. Clim. Change* https://doi.org/10.1038/s41558-024-02234-5 (2025).
44. Aerts, R. The freezer defrosting: global warming and litter decomposition rates in cold biomes. *J. Ecol.* **94**, 713–724 (2006).
45. Wang, N. et al. Effects of climate warming on carbon fluxes in grasslands—a global meta-analysis. *Glob. Change Biol.* **25**, 1839–1851 (2019).
46. Urban, M. C. Climate change extinctions. *Science* **386**, 1123–1128 (2024).
47. Huang, M. et al. Air temperature optima of vegetation productivity across global biomes. *Nat. Ecol. Evol.* **3**, 772–779 (2019).
48. Elrys, A. S. et al. Aridity creates global thresholds in soil nitrogen retention and availability. *Glob. Change Biol.* **30**, e17003 (2023).
49. Wuepper, D., Borrelli, P. & Finger, R. Countries and the global rate of soil erosion. *Nat. Sustain.* **3**, 51–55 (2019).

50. Wu, Q. et al. Contrasting effects of altered precipitation regimes on soil nitrogen cycling at the global scale. *Glob. Change Biol.* **28**, 6679–6695 (2022).
51. Stocker, B. D. et al. Drought impacts on terrestrial primary production underestimated by satellite monitoring. *Nat. Geosci.* **12**, 264–270 (2019).
52. Mahecha, M. et al. Biodiversity loss and climate extremes—study the feedbacks. *Nature* **612**, 30–32 (2022).
53. Sun, J. et al. Biocrusts modulate carbon losses under warming across global drylands: a Bayesian meta-analysis. *Soil Biol. Biochem.* **188**, https://doi.org/10.1016/j.soilbio.2023.109214 (2024).
54. Wang, B. et al. Differential effects of altered precipitation regimes on soil carbon cycles in arid versus humid terrestrial ecosystems. *Glob. Change Biol.* **27**, 6348–6362 (2021).
55. Zhou, Z., Wang, C. & Luo, Y. Meta-analysis of the impacts of global change factors on soil microbial diversity and functionality. *Nat. Commun.* **11**, 3072 (2020).
56. Garland, G. et al. A closer look at the functions behind ecosystem multifunctionality: a review. *J. Ecol.* **109**, 600–613 (2020).
57. Grass, I. et al. Trade-offs between multifunctionality and profit in tropical smallholder landscapes. *Nat. Commun.* **11**, 1186 (2020).
58. Giling, D. P. et al. A niche for ecosystem multifunctionality in global change research. *Glob. Change Biol.* **25**, 763–774 (2019).
59. Le Bagousse-Pinguet, Y. et al. Phylogenetic, functional, and taxonomic richness have both positive and negative effects on ecosystem multifunctionality. *Proc. Natl Acad. Sci. USA* **116**, 8419–8424 (2019).
60. Xiao, L. et al. Global depth distribution of belowground net primary productivity and its drivers. *Glob. Ecol. Biogeogr.* **32**, 1435–1451 (2023).
61. Spawn, S. A., Sullivan, C. C., Lark, T. J. & Gibbs, H. K. Harmonized global maps of above and belowground biomass carbon density in the year 2010. *Sci. Data* **7**, https://doi.org/10.1038/s41597-020-0444-4 (2020).
62. Poggio, L. et al. SoilGrids 2.0: producing soil information for the globe with quantified spatial uncertainty. *Soil* **7**, 217–240 (2021).
63. He, X. et al. Global patterns and drivers of soil total phosphorus concentration. *Earth Syst. Sci. Data* **13**, 5831–5846 (2021).
64. McDowell, R. W., Noble, A., Pletnyakov, P. & Haygarth, P. M. A global database of soil plant available phosphorus. *Sci. Data* **10**, https://doi.org/10.1038/s41597-023-02022-4 (2023).
65. Guo, Z. et al. Soil dissolved organic carbon in terrestrial ecosystems: global budget, spatial distribution and controls. *Glob. Ecol. Biogeogr.* **29**, 2159–2175 (2020).
66. Xu, X., Thornton, P. E. & Post, W. M. A global analysis of soil microbial biomass carbon, nitrogen and phosphorus in terrestrial ecosystems. *Glob. Ecol. Biogeogr.* **22**, 737–749 (2013).
67. Xu, R. I. & Prentice, I. C. Terrestrial nitrogen cycle simulation with a dynamic global vegetation model. *Glob. Change Biol.* **14**, 1745–1764 (2008).
68. Xu, R., Prentice, I. C., Spahni, R. & Niu, H. S. Modelling terrestrial nitrous oxide emissions and implications for climate feedback. *N. Phytol.* **196**, 472–488 (2012).
69. Colin, P. I. J. B. Modelling the demand for new nitrogen fixation by terrestrial ecosystems. *Biogeosciences* **14**, 2003–2017 (2017).
70. Fick, S. E. & Hijmans, R. J. WorldClim 2: new 1-km spatial resolution climate surfaces for global land areas. *Int. J. Climatol.* **37**, 4302–4315 (2017).
71. Panagos, P. et al. European Soil Data Centre 2.0: soil data and knowledge in support of the EU policies. *Eur. J. Soil Sci.* **73**, e13315 (2022).
72. Ellis, E. C., Antill, E. C. & Kreft, H. All is not loss: plant biodiversity in the Anthropocene. *PLoS ONE* **7**, e30535 (2012).
73. Beck, H. E. et al. Present and future Koppen–Geiger climate classification maps at 1-km resolution. *Sci. Data* **5**, https://doi.org/10.1038/sdata.2018.214 (2018).
74. Manning, P. et al. Redefining ecosystem multifunctionality. *Nat. Ecol. Evol.* **2**, 427–436 (2018).
75. Gross, N. et al. Functional trait diversity maximizes ecosystem multifunctionality. *Nat. Ecol. Evol.* **1**, https://doi.org/10.1038/s41559-017-0132 (2017).
76. Abdi, H. & Williams, L. J. Principal component analysis. *Wiley Interdiscip. Rev.: Comput. Stat.* **2**, 433–459 (2010).
77. Meyer, S. T. et al. Biodiversity-multifunctionality relationships depend on identity and number of measured functions. *Nat. Ecol. Evol.* **2**, 44–49 (2018).
78. Gamfeldt, L., Hillebrand, H. & Jonsson, P. R. Multiple functions increase the importance of biodiversity for overall ecosystem functioning. *Ecology* **89**, 1223–1231 (2008).
79. Dooley, A. et al. Testing the effects of diversity on ecosystem multifunctionality using a multivariate model. *Ecol. Lett.* **18**, 1242–1251 (2015).
80. Byrnes, J. E. K. et al. Investigating the relationship between biodiversity and ecosystem multifunctionality: challenges and solutions. *Methods Ecol. Evol.* **5**, 111–124 (2014).
81. Yao, Y. et al. Spatiotemporal pattern of gross primary productivity and its covariation with climate in China over the last thirty years. *Global Change Biol.* **24**, https://doi.org/10.1111/gcb.13830 (2017).
82. Migliavacca, M. et al. The three major axes of terrestrial ecosystem function. *Nature* **598**, 468–472 (2021).
83. Bernardino, P. N. et al. Predictability of abrupt shifts in dryland ecosystem functioning. *Nat. Clim. Change* **15**, 86–91 (2025).
84. Mo, L. et al. Integrated global assessment of the natural forest carbon potential. *Nature* **624**, 92–101 (2023).
85. Yu, Y. et al. Machine learning-based observation-constrained projections reveal elevated global socioeconomic risks from wildfire. *Nat. Commun.* **13**, 1250 (2022).
86. O'Neill, B. et al. The Scenario Model Intercomparison Project (ScenarioMIP) for CMIP6. *Geosci. Model Dev.* **9**, 3461–3482 (2016).

Acknowledgements

This study was supported by the Science and Technology Projects of Xizang Autonomous Region, China (XZ202501ZY0091), the Ecological Conservation and High Quality Development of the Yellow River Basin Program, China (2022-YRUC-01 0102), the National Science Foundation of China (Grant No. 42301071), the Key Laboratory of Biodiversity and Environment on the Qinghai-Tibet Plateau, Ministry of Education (KLBE2025009), the Key Laboratory of Forest Ecology of Xizang Plateau, Ministry of Education (XZAJYBSYS-202501), the China Postdoctoral Science Foundation (Grant No. 2023M743633). JP was funded by the Spanish Government grants PID2022-140808NB-I00, and TED2021-132627 B-I00 funded by MCIN, AEI/10.13039/501100011033 European Union Next Generation EU/PRTR. We also thank W. He, Y. Hu, and R. Xu for their help with data extraction and comments on earlier manuscript versions. Thank the support from the Tibet Research Academy of Eco-environmental Sciences, Tibet Autonomous Region; College of Grassland, Resources and Environment, Key Laboratory of Grassland Resources of the Ministry of Education of China, Inner Mongolia Agricultural University.

Author contributions

All authors contributed to the paper. J.S. contributed to the conceptualization. T.C.Z. wrote the original draft. T.C.Z., J.S., C.C.Y., X.J., E.Y.L., X.Y.L., A.S.M., M.E.M., and J.P. contributed to the methodology, formal analysis, data curation, software, review, editing, and visualization.

https://doi.org/10.1038/s41467-025-64453-4

Competing interests
The authors declare no competing interests.

Additional information
Supplementary information The online version contains supplementary material available at https://doi.org/10.1038/s41467-025-64453-4.

Correspondence and requests for materials should be addressed to Jian Sun.

Peer review information *Nature Communications* thanks Anton Potapov and the other, anonymous, reviewer(s) for their contribution to the peer review of this work. A peer review file is available.

Reprints and permissions information is available at http://www.nature.com/reprints

Publisher's note Springer Nature remains neutral with regard to jurisdictional claims in published maps and institutional affiliations.